Structural and Magnetic Properties of $Mn_{1-t}Cr_tAs_{1-x}P_x$

Helmer Fjellvåg,[a] Arne Kjekshus,[a,*] Svein Stølen[a] and Arne F. Andresen[b]

[a]Department of Chemistry, University of Oslo, Blindern, N-0315 Oslo 3 and [b]Institute for Energy Technology, N-2007 Kjeller, Norway

Fjellvåg, H., Kjekshus, A., Stølen, S. and Andresen, A. F., 1988. Structural and Magnetic Properties of $Mn_{1-t}Cr_tAs_{1-x}P_x$. – Acta Chem. Scand., Ser. A 42: 214–225.

$Mn_{1-t}Cr_tAs_{1-x}P_x$ has been investigated for $0.00 < t < 1.00$ and $0.00 < x < 0.20$ by X-ray and neutron diffraction, magnetic susceptibility and DTA measurements. Apart from a narrow composition region near MnAs where the atoms are in a "high"-spin state, $Mn_{1-t}Cr_tAs_{1-x}P_x$ generally adopts the orthorhombic MnP-type structure with "low"-spin Mn below a second-order transition temperature T_D. Above T_D it adopts the hexagonal NiAs-type structure and "high"-spin Mn prevails. The lowest T_D values are found near MnAs, and T_D increases approximately linearly with t and x according to the empirical relation $T_D(t,x) \approx (390 + \delta_T \cdot t + \delta_X)$K where $\delta_T = 783$ and $\delta_X = 730$. The magnetic susceptibility follows the Curie-Weiss law above T_D and the effective moment obeys the empirical relation $\mu(t) \approx \mu_{Mn} \cdot (1-t) + \mu_{Cr} \cdot t$ with $\mu_{Mn} = 4.62\ \mu_B$ and $\mu_{Cr} = 2.90\ \mu_B$ (independent of x). The anomalous behaviour of the magnetic susceptibility below T_D originates from the gradual spin conversion which accompanies the NiAs ⇄ MnP-type phase transition. Different heli- and ferromagnetic arrangements occur at low temperature, depending on t, x and T. The general effect of the substitution of P for As is to favour ferromagnetism in the MnP-type phase at low temperature. The detailed exploration of the heli- and ferromagnetic structures are, for some of the samples, hampered by non-random distributions within the metal and/or non-metal sub-lattices.

A number of recent papers from this Institute have been devoted to the intriguing structural and magnetic properties of the solid-solution phases $Mn_{1-t}Cr_tAs$[1-6] and $MnAs_{1-x}P_x$.[7-12] As a function of various parameters, such as composition (x or t), temperature (T), pressure (p) and magnetic field (H), several structural and magnetic phase transitions take place. The crystal structure is of either MnP- or NiAs-type, whereas different ferro- and helimagnetic spin arrangements appear at low temperatures.[1,2,4-9,12] In the paramagnetic temperature region a continuous spin conversion between "low"- and "high"-spin manganese occurs, and this phenomenon is particularly well documented (cf. Refs. 7, 9-12 and references therein) for $MnAs_{1-x}P_x$, where the conversion process is also accompanied by large anomalies in heat capacity and magnetic susceptibility.

A common feature for most binary MnP- and NiAs-type phases is their ability to form extended ternary solid-solution phases. Although little information is presently at hand, it seems likely that these phases are capable of forming solid-solution phases with an even larger number of constituents than three. The present contribution concerns the quaternary $Mn_{1-t}Cr_tAs_{1-x}P_x$ phase, thereby combining the interesting properties of $MnAs_{1-x}P_x$ and $Mn_{1-t}Cr_tAs$ in a quaternary phase. The present work embraces samples with a rather low phosphorus content, $0.00 < x < 0.20$, and describes results obtained by powder X-ray and neutron diffraction, magnetic susceptibility and differential thermal analysis (DTA) measurements.

Experimental

The syntheses of the quaternary $Mn_{1-t}Cr_tAs_{1-x}P_x$ samples were performed in three steps following

*To whom correspondence should be addressed.

the sealed, evacuated silica-glass technique. First, batches of CrP, CrAs, MnP and MnAs were prepared using the pure elements as starting materials according to the procedures given in Refs. 1 and 7. Secondly, ternary samples of $MnAs_{1-x}P_x$ and $CrAs_{1-x}P_x$ were synthesized by heating stoichiometric quantities of the binary phases. These samples were subjected to one heat treatment at 900 °C for two weeks and then, after intermediate grinding, re-annealed twice at 800 °C for two weeks before being slowly cooled to room temperature over a period of one day. In the third step, the syntheses of the quaternary samples from the ternary intermediates followed the same course as in the second step.

Various experimental details regarding the powder X-ray and neutron diffraction experiments and data reduction, magnetic susceptibility and DTA measurements are given in Refs. 1, 7 and 9. In the Rietveld refinements [13,14] of the powder neutron diffraction data, the nuclear scattering lengths $b_{Mn} = -3.73$, $b_{Cr} = 3.635$, $b_{As} = 6.58$ and $b_P = 5.13$ fm were taken from Ref. 15. The magnetic form factors for Mn^{2+} and Cr^{3+} from Ref. 16 were adopted in calculations involving cooperative magnetic arrangements.

Results and discussion

(i) Solid solution and atomic arrangement. The ternary MnAs–CrAs system exhibits complete solid solubility. This characteristic is retained on turning to the phosphorus-substituted samples $Mn_{1-t}Cr_tAs_{1-x}P_x$ with $0.00 < x < 0.20$. At higher substitution levels of phosphorus a two-phase region develops within the ternary $MnAs_{1-x}P_x$ phase,[17,18] but the present work does not examine how far into the quaternary system the two-phase region extends. A schematic illustration showing the structural and magnetic situation at low temperatures (say 10 K) is presented in Fig. 1. Samples with composition close to MnAs adopt the NiAs-type structure and are ferromagnetic ($\mu_F \approx 3.4\ \mu_B$)[19] below room temperature. The rest of the single-phase region in Fig. 1 adopts the MnP-type structure [in para- (P), ferro- (F) and helimagnetic (H) states] at and below room temperature.

Fig. 2 shows the variations in the unit cell dimensions (*Pnma* setting of the MnP-type unit cell) of $Mn_{1-t}Cr_tAs_{1-x}P_x$ with t (at 295 K) for the fixed values of $x = 0.05$, 0.10, 0.12 and 0.14. The observed Bragg reflections in the powder X-ray

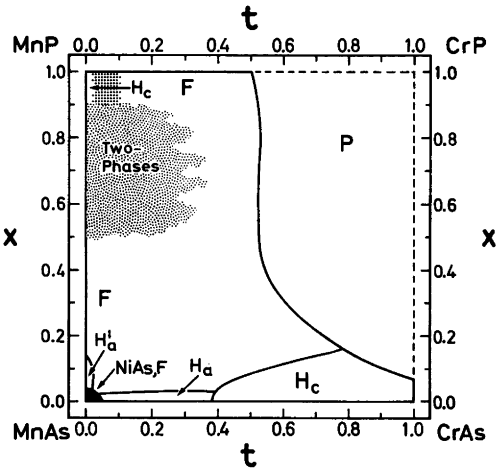

Fig. 1. Schematic phase diagram for $Mn_{1-t}Cr_tAs_{1-x}P_x$ (at ~10 K). Abbreviations for magnetic states are F, ferro-, H_a, heli- with propagation along *a*, H_c, heli- with propagation along *c*, and P, paramagnetic.

and neutron diffraction diagrams are all sharp, and no additional reflections were observed. This establishes that Mn and Cr are randomly (long range) distributed over the metal sub-lattice, and P and As similarly over the non-metal sub-lattice. The V versus t curve for $x = 0.05$ differs somewhat from those for $x = 0.10$, 0.12 and 0.14. This is more clearly seen from Fig. 3, which shows the deviation $[\Delta V(t)]$ from a Vegard law relationship for $x = 0.05$ and 0.10. The curve for $x = 0.05$ is nearly antisymmetric around $t = 0.50$, while the corresponding curve for $x = 0.10$ is almost symmetric. The distinction between these curves is probably rooted in the different spin states for manganese at the two ternary $MnAs_{1-x}P_x$ end compositions. For $MnAs_{0.95}P_{0.05}$ manganese is in a "high"-spin state at room temperature, whereas for $MnAs_{0.90}P_{0.10}$ it adopts a lower spin state.[7,9–12] The spin value, and thereby also the effective size of the manganese atoms,[19,20] is, for $x = 0.05$, clearly lowered upon substitution of chromium, whereas corresponding, significant perturbations cannot take place for $x = 0.10$ (cf. Figs. 2a, b and note the different curve shapes for $0.00 < t < 0.20$). The large changes in the electronic band structure associated with these spin and size adjustments may explain why e.g. samples of $Mn_{1-t}Cr_tAs_{0.95}P_{0.05}$ with $0.00 < t < 0.10$ turned out to be rather difficult to anneal to a single-phase state.

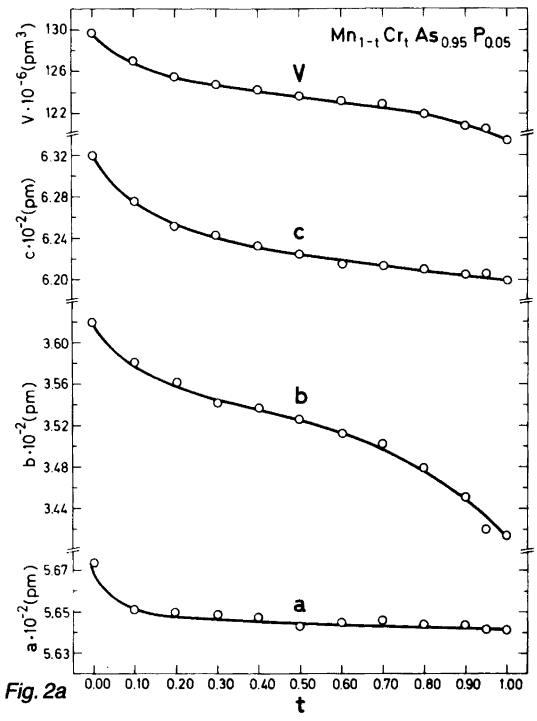

Fig. 2a

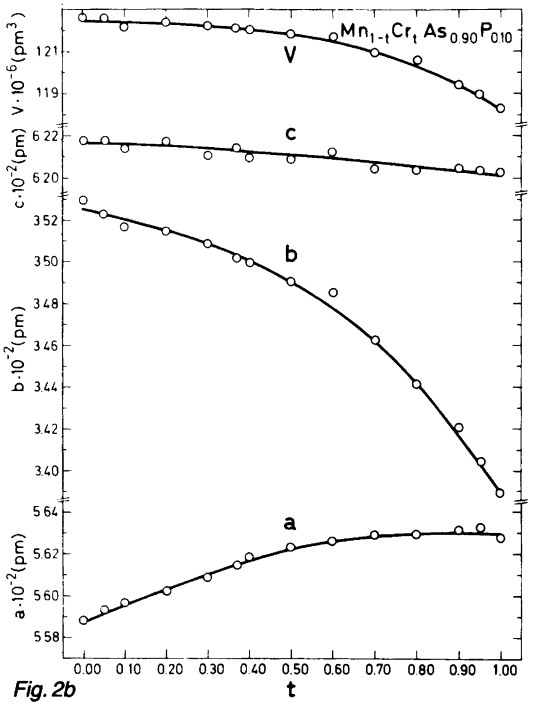

Fig. 2b

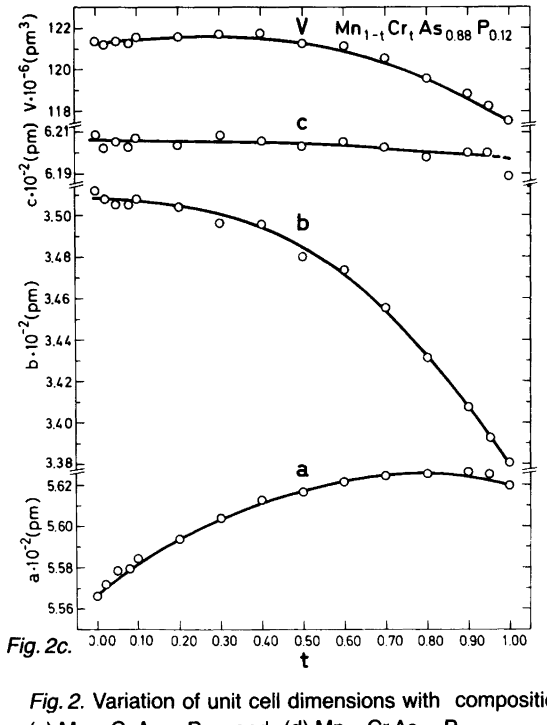

Fig. 2c.

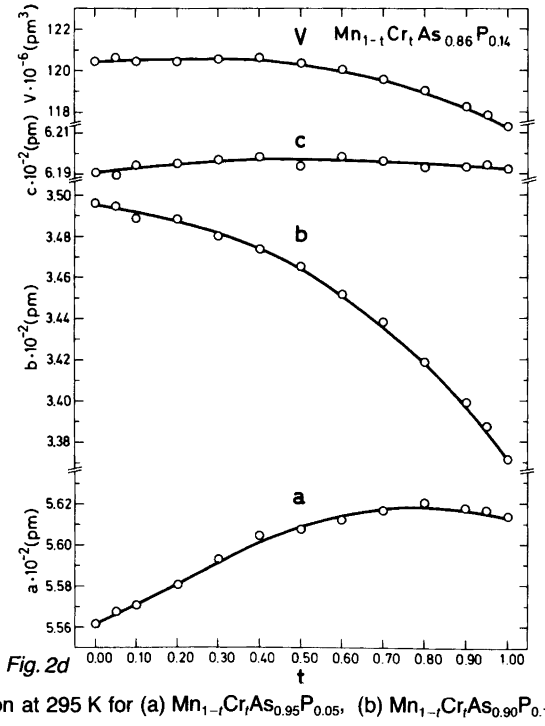

Fig. 2d

Fig. 2. Variation of unit cell dimensions with composition at 295 K for (a) $Mn_{1-t}Cr_tAs_{0.95}P_{0.05}$, (b) $Mn_{1-t}Cr_tAs_{0.90}P_{0.10}$, (c) $Mn_{1-t}Cr_tAs_{0.88}P_{0.12}$ and (d) $Mn_{1-t}Cr_tAs_{0.86}P_{0.14}$.

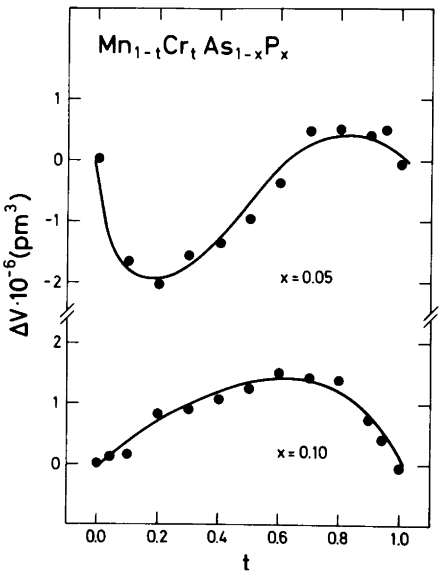

Fig. 3. Variation of deviation in unit cell volume (ΔV) from Vegard's law relationship for $Mn_{1-t}Cr_tAs_{0.95}P_{0.05}$ and $Mn_{1-t}Cr_tAs_{0.90}P_{0.10}$.

Positional parameters for various samples of $Mn_{1-t}Cr_tAs_{1-x}P_x$ were derived from powder neutron diffraction data by profile refinement according to the Rietveld method,[13] and the results are listed in Table 1 for temperatures at and below room temperature. Together with low-temperature X-ray diffraction data these results confirm that except for a narrow composition range close to MnAs, the atomic arrangement is of the MnP type at T < 295 K. Representative examples of thermal expansion curves for $100 \leq T \leq 300$ K are shown in Figs. 4a–d. Samples with t and x close to zero show behaviour similar to that of MnAs[20–22] in that they undergo a first-order, coupled structural and magnetic phase transition from an MnP,P- to NiAs,F-type phase upon cooling. $T_{C,i}$ = 317 K for MnAs,[21] and is lowered to 281 and 302 K for $MnAs_{0.97}P_{0.03}$ and $Mn_{0.97}Cr_{0.03}As$, respectively, whereas $T_{C,i}$ = 295 K for the quaternary sample $Mn_{0.99}Cr_{0.01}As_{0.99}P_{0.01}$.

For quaternary samples with $\sim 0.03 < x < 0.20$ and $\sim 0.02 < t < \sim 0.40$ only continuous changes in the unit cell dimensions were observed below room temperature (cf. Figs. 4a–c). Hence, the magnetic order–disorder and order–order transitions which occur in these composition ranges are not connected with any easily detectable discontinuities in the thermal expansion characteristics. For $Mn_{1-t}Cr_tAs$ (i.e. no phosphorus present) the magnetic disorder–order transition between P and H_a (index gives the crystallographic orientation of the propagation direction of the spirals) states is of first order,[1,2] but the transition converts into second-order for $x > \sim 0.03$, the quaternary region.

In a narrow composition range of $Mn_{1-t}Cr_tAs$ around $t \approx 0.35$ a first-order structural and magnetic phase transition between two helimagnetic phases (H_a and H_c) takes place at T_S.[1,2] The difference in stability between these helimagnetic phases as well as their stability with respect to ferromagnetism is strongly affected by small changes in chemical and physical variables.[1–9,20,21] Low-temperature X-ray diffraction data for sam-

Table 1. Unit cell dimensions (in 10^2 pm = Å) and positional parameters with standard deviations for $Mn_{1-t}Cr_tAs_{0.88}P_{0.12}$ as derived by Rietveld analysis of powder neutron diffraction data. Space group *Pnma*; Mn/Cr in 4*c* and As/P in 4*c* (nuclear R_n factors ranging between 0.03 and 0.07, profile R_p factors ranging between 0.10 and 0.14, 25–30 reflections).

t	T/K	a	b	c	x_{Mn}/Cr	z_{Mn}/Cr	x_{As}/P	z_{As}/P
0.02	293	5.5718(3)	3.5040(2)	6.1997(4)	0.0105(25)	0.2125(25)	0.1997(12)	0.5806(12)
	225	5.5360(3)	3.4663(2)	6.1497(4)	0.0067(24)	0.1978(24)	0.1996(11)	0.5780(12)
	120	5.5147(3)	3.4483(2)	6.1151(4)	0.0072(12)	0.1940(14)	0.1943(6)	0.5768(7)
	10	5.5105(3)	3.4467(2)	6.1093(4)	0.0062(21)	0.1970(18)	0.1972(10)	0.5770(11)
0.04	293	5.5736(4)	3.5040(3)	6.1995(5)	0.0082(30)	0.2032(14)	0.2073(26)	0.5890(13)
	10	5.5124(3)	3.4458(2)	6.1119(4)	0.0069(11)	0.1941(6)	0.2047(9)	0.5808(6)
0.10	293	5.5891(2)	3.5190(2)	6.2161(3)	0.0068(20)	0.2133(20)	0.2051(7)	0.5801(8)
	10	5.5249(2)	3.4491(1)	6.1242(3)	0.0047(9)	0.1996(7)	0.1969(4)	0.5782(4)

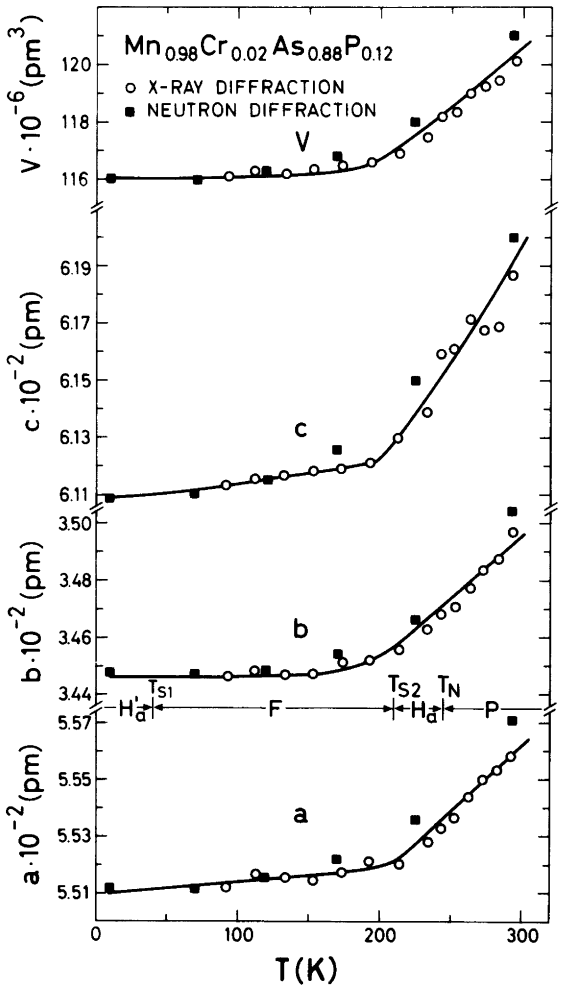

Fig. 4a

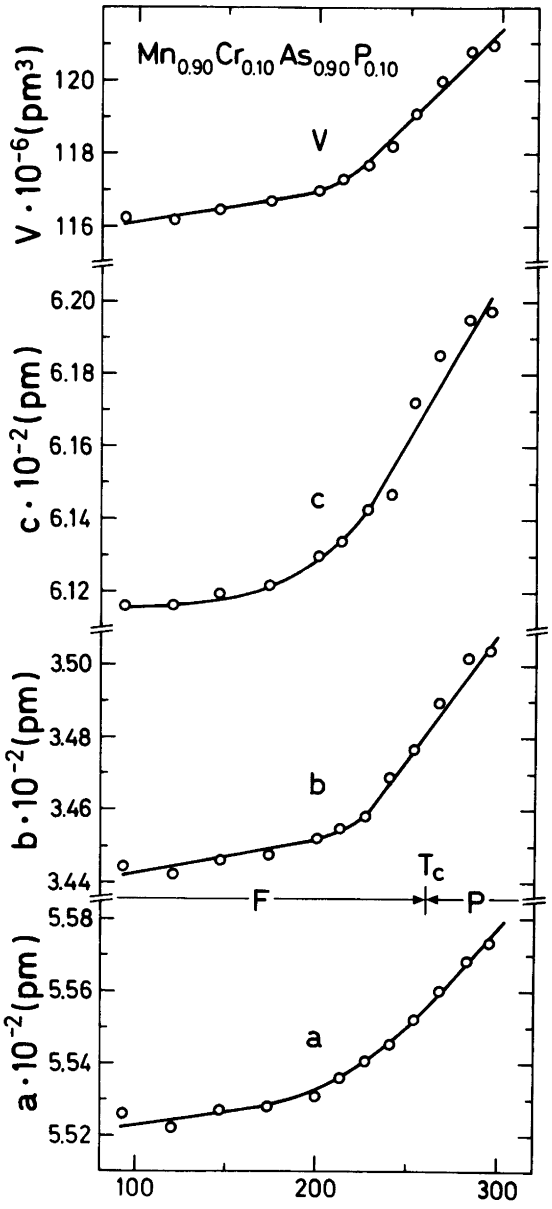

Fig. 4b

Fig. 4. Variation of unit cell dimensions below room temperature for (a) $Mn_{0.98}Cr_{0.02}As_{0.88}P_{0.12}$, (b) $Mn_{0.90}Cr_{0.10}As_{0.90}P_{0.10}$, (c) $Mn_{0.70}Cr_{0.30}As_{0.88}P_{0.12}$ and (d) $Mn_{0.63}Cr_{0.37}As_{0.995}P_{0.005}$. Magnetic states and transition temperatures are indicated on the figures.

ples from this region of the quaternary phase show that T_S increases with increasing x (cf. Fig. 4d). A detailed account of the findings for $Mn_{0.64}Cr_{0.36}As_{1-x}P_x$ and $Mn_{0.63}Cr_{0.37}As_{1-x}P_x$ will be published separately.

The orthorhombic distortion decreases continuously with increasing temperature and the MnP-type structure transforms into the NiAs-type at T_D. The lowest values of T_D are found for compositions close (and equal) to MnAs.[2,7] T_D increases approximately linearly with the substitution parameter t or x; $\delta_T = \Delta T_D/\Delta t = 783$ K for

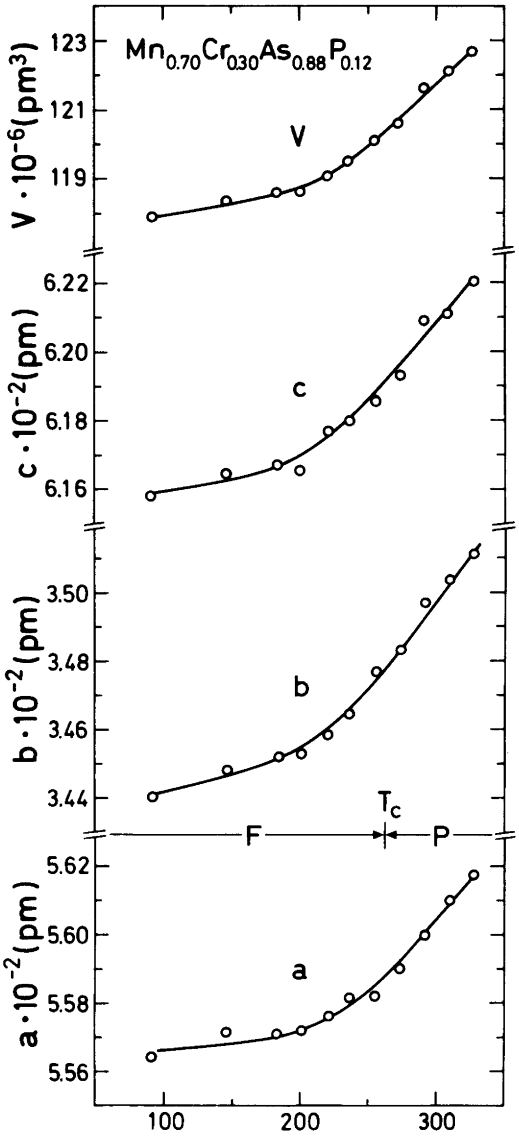

Fig. 4c.

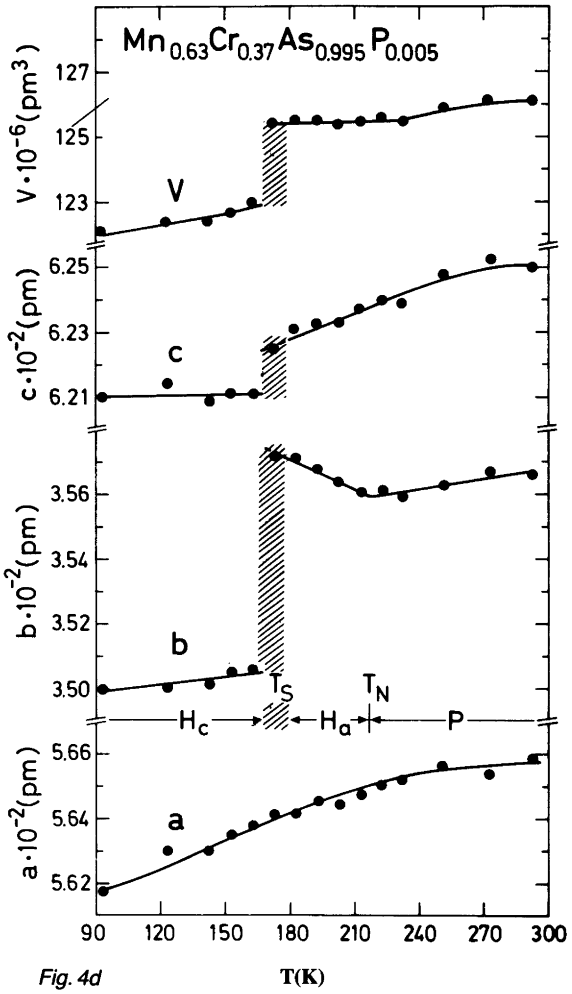

Fig. 4d

$Mn_{1-t}Cr_tAs$ and $\delta_x = \Delta T_D/\Delta x \approx 730$ K for $MnAs_{1-x}P_x$ ($x < 0.20$). These simple additivity relations extend into the quaternary phase where $T_D(T,x) \approx 390$ K $+ \delta_T \cdot t + \delta_x \cdot x$ describes the measured T_D values for some 50 different samples with $0.00 < t < 0.50$ and $0.00 < x < 0.20$ to a fairly good approximation. Representative examples showing the temperature dependence of the unit cell dimensions for quaternary samples undergoing the MnP ⇄ NiAs-type transition are given in Fig. 5. The thus obtained values for T_D agree well with those derived from magnetic susceptibility and DTA measurements (see below).

(ii) Paramagnetic properties. For temperatures above T_D the magnetic susceptibility of $Mn_{1-t}Cr_tAs_{1-x}P_x$ with $0.00 \leq t \leq 1.00$ and $0.00 \leq x < 0.20$ is found to obey the Curie-Weiss law. Values for the paramagnetic moment $\mu_{eff} = \sqrt{8C_{mol}}$ and the Weiss constant θ are given in Table 2. For a given Mn:Cr atomic ratio (i.e. a fixed value of t) μ_{eff} does not change significantly with variation of x within $0.05 \leq x \leq 0.14$,

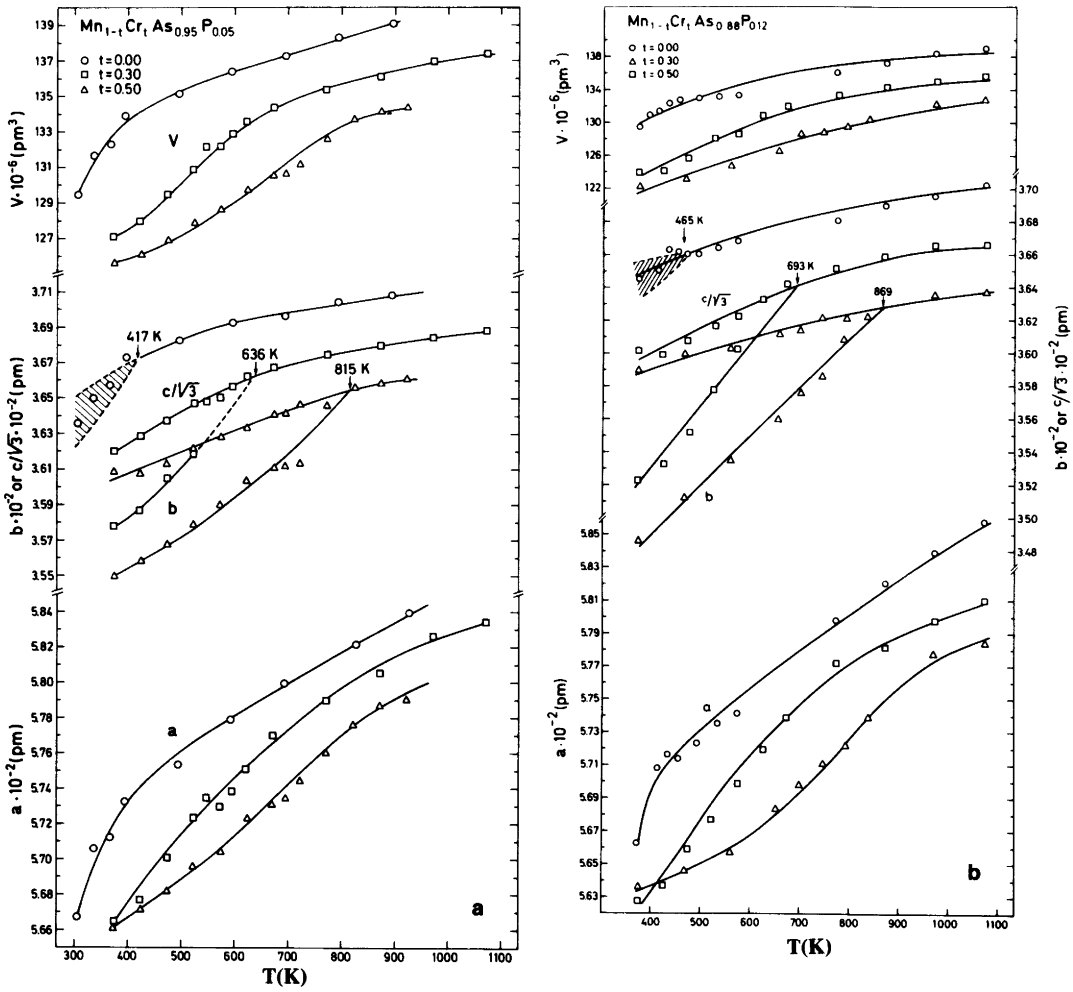

Fig. 5. Variation of unit cell dimensions with temperature between 300 and 1100 K for (a) $Mn_{1-t}Cr_tAs_{0.95}P_{0.05}$ with $t = 0.00$, 0.30 and 0.50, (b) $Mn_{1-t}Cr_tAs_{0.88}P_{0.12}$ with $t = 0.00$, 0.30 and 0.50. The hatched regions for $c/\sqrt{3}$ and b for $t = 0.00$ refer to assessments based on line-broadening of relevant reflections.

whereas θ decreases with increasing phosphorus content. Earlier reports give rather varying values for μ_{eff} in $MnAs_{1-x}P_x$, e.g. μ_{eff} = 4.08–4.24 μ_B[18] for x = 0.05–0.20, μ_{eff} = 4.6 μ_B[9,10] for x = 0.06–0.18, μ_{eff} = 5.0 μ_B[23] for x = 0.075, μ_{eff} = 3.7 μ_B[24] and 4.59 μ_B[25] for x = 0.08, μ_{eff} = 4.87 μ_B[26] and 5.0 μ_B[27] for x = 0.10, and μ_{eff} = 4.45–4.55 μ_B[7] for x = 0.12–0.18. The present results (Table 2) for t = 0.00 and $0.05 \leq x < 0.20$ fit well with those of Refs. 7, 9, 10 and 25.

The substitution of Cr for Mn involves a decrease in μ_{eff}, whereas only a slight and irregular variation in θ is observed. For $Mn_{1-t}Cr_tAs_{1-x}P_x$ with $0.05 \leq x \leq 0.14$ it is possible to describe μ_{eff} as a sum of manganese and chromium paramagnetic moments, viz. $\mu(t) \approx \mu_{Mn}\cdot(1-t) + \mu_{Cr}$.with μ_{Mn} = 4.62 μ_B and μ_{Cr} = 2.90 μ_B, in which x does not appear. The values for Mn (viz. MnAs) and Cr (viz. CrAs) fit reasonably well with μ_{eff} = 4.95 μ_B observed for MnAs and the extrapolated value for CrAs μ_{eff} = 3.2 μ_B.[28] It should be emphasized that the obeyance of such an additivity relation does not imply that the question of localized versus delocalized Mn and Cr moments can be settled.

In the temperature range below T_D, where the

Table 2. Paramagnetic moment (μ_{eff}) and Weiss constant (θ) with standard deviations for the NiAs-type state of $Mn_{1-t}Cr_tAs_{1-x}P_x$. The final column gives magnetic moments from $\mu = \mu_{Mn} \cdot (1-t) + \mu_{Cr} \cdot t$ with $\mu_{Mn} = 4.62$ μ_B and $\mu_{Cr} = 2.90$ μ_B.

t	$x = 0.05$		$x = 0.10$		$x = 0.12$		$x = 0.14$		Calculated
	μ_{eff}/μ_B	θ/K	μ_{eff}/μ_B	θ/K	μ_{eff}/μ_B	θ/K	μ_{eff}/μ_B	θ/K	μ/μ_B
0.00	4.50(1)	210(4)	4.63(4)	130(12)	4.60(3)	110(8)	4.65(6)	64(19)	4.62
0.05	4.52(2)	195(5)	4.56(3)	107(8)	4.52(2)	97(7)	4.56(7)	67(20)	4.53
0.10	4.44(2)	185(5)	4.42(4)	135(4)	4.44(2)	91(8)	4.38(8)	108(25)	4.45
0.20	4.31(2)	185(7)	4.33(4)	128(14)	4.25(4)	114(14)	4.44(8)	83(88)	4.28
0.30	4.24(3)	139(13)	4.15(4)	127(18)	4.09(4)	147(15)	4.07(10)	135(32)	4.11
0.40	3.81(2)	217(10)	3.90(5)	169(22)	3.91(10)	162(43)	4.00(12)	118(50)	3.93
0.50	3.70(9)	198(44)	3.84(15)	120(71)	3.93(11)	118(56)	3.64(14)	198(70)	3.76

MnP-type deformation progresses continuously, anomalous paramagnetic susceptibility behaviour is observed (cf. Figs. 6a, b). For the ternary $MnAs_{1-x}P_x$ end compositions the anomalous $\chi(T)$ behaviour has a counterpart in a broad, but marked peak in the heat-capacity (C_p) curves (cf. Refs. 9, 11 and 12, and references therein). Such pronounced C_p anomalies are not found for $Mn_{1-t}Cr_tAs$, and those for $MnAs_{1-x}P_x$ fade rapidly away on substitution of Cr for Mn. Recently, several pieces of experimental evidence have become available which make a phenomenological interpretation of the C_p observations possible.[11,12] A very large and strongly temperature-dependent thermal expansion (together with a corresponding anomalous behaviour of the isothermal compressibility) gives rise to extraordinarily large dilational contributions to the heat capacity and this, in turn, accounts for the C_p anomaly. Paramagnetic diffuse scattering experiments on $MnAs_{1-x}P_x$ with $0.06 \leq x \leq 0.18$ have shown that a continuous reduction of the spin value S is coupled to the progressing structural MnP-type distortion.[10] Thus, the anomalous susceptibility behaviour displayed in Fig. 6 can quantitatively also be accounted for as an effect of a gradual spin conversion, possibly modified by changes in the overall magnetic exchange resulting from changes in the metal–metal interactions brought about by the substitution of Cr for Mn.

(iii) Cooperative magnetism. Neutron diffraction data at and below room temperature were collected for $Mn_{1-t}Cr_tAs_{0.88}P_{0.12}$ with $t = 0.02$, 0.04, 0.10 and 0.30. The ternary end composition $MnAs_{0.88}P_{0.12}$ shows very complicated cooperative magnetic properties.[7–12] For $T < T_{S1} = 60 \pm 10$ K helimagnetic order (modified Ha type, denoted H_a') is observed, for $T_{S1} < T < T_{S2} = 200 \pm 10$ K ferromagnetism with magnetic moments parallel to the b_{MnP} axis is found, while for $T_{S2} < T < T_N = 234.1$ K ($T_N = 240 \pm 5$ K by powder neutron diffraction[9]) helimagnetic order (H_a type) again prevails.[7–12] On further increase in the phosphorus content the ferromagnetic region grows at the expense of the helimagnetic regions. The main effect of the P substitution is to reduce the unit cell volume, and it is hence quite reasonable that the x,T phase diagram for $MnAs_{1-x}P_x$ turns out to be quite analogous to the p,T phase diagram for MnAs.[20] The observed magnetic moments for the ordered F, H_a and H_a' MnP-type phases correspond to a "low"-spin state for manganese.

Upon increasing chromium substitution in $Mn_{1-t}Cr_tAs_{0.88}P_{0.12}$, ferromagnetism is favoured. The temperature dependence of the integrated intensity of the 000^r satellite reflection, being characteristic of the incommensurate helimagnetic order, is shown for $t = 0.02$ in Fig. 7. From this figure it is seen that the intermediate temperature interval for the ferromagnetic state has expanded, T_{S1}, T_{S2} and T_N being now 40 ± 10, 210 ± 10 and 245 ± 10 K, respectively. For $t = 0.04$ the H_a'- and H_a-type arrangements are still observed ($T_{S1} = 40 \pm 10$ K, $T_{S2} = 210 \pm 10$ K, $T_N = 255 \pm 10$ K), while for $t \geq 0.10$ the ferromagnetism has completely taken over. The magnetic order–disorder temperature decreases only slightly with increasing chromium content: from $T_C = 234.1$ K for $t = 0.00$ to $T_C = 255$ and 260 K for $t = 0.10$ and 0.30, respectively. T_C as assessed from DTA gradually becomes more difficult to

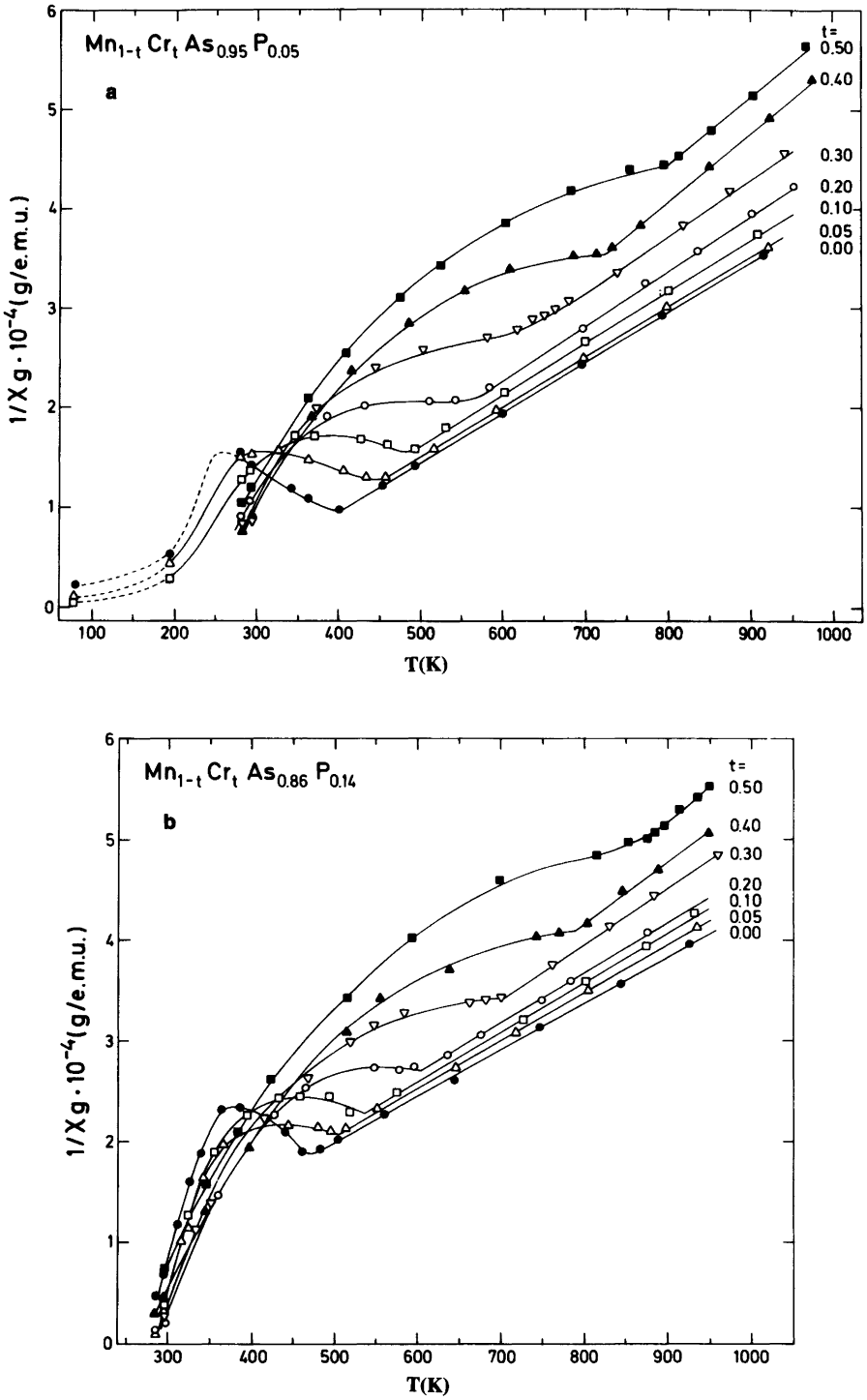

Fig. 6. Inverse magnetic susceptibility versus temperature for (a) $Mn_{1-t}Cr_tAs_{0.95}P_{0.05}$ and (b) $Mn_{1-t}Cr_tAs_{0.86}P_{0.14}$.

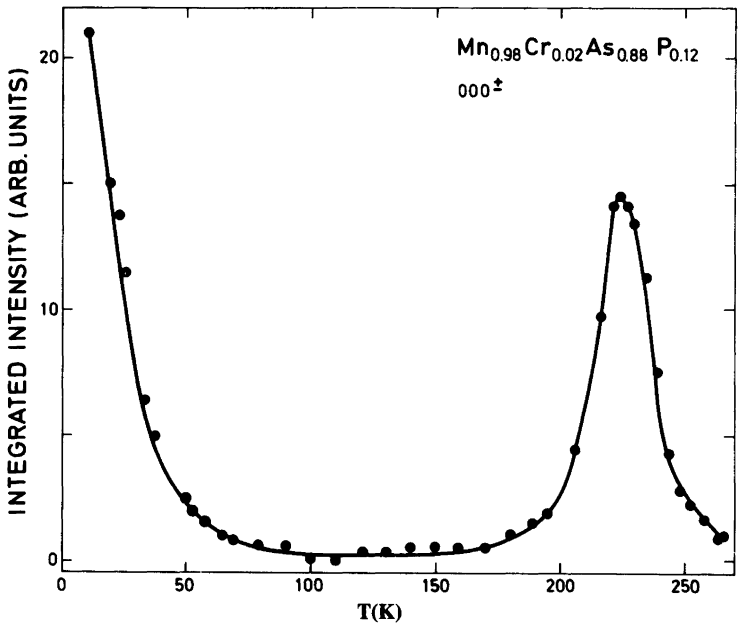

Fig. 7. Temperature dependence of the integrated intensity of $000^{\pm}$ for $Mn_{0.98}Cr_{0.02}As_{0.88}P_{0.12}$. A slightly temperature shifted, but otherwise identical $000^{\pm}$ characteristic is obtained for $Mn_{0.96}Cr_{0.04}As_{0.88}P_{0.12}$.

detect for $t > 0.30$ due to diminishing and/or blurring of the associated C_p peak. This probably reflects decrease in the magnetic moment, weakening of the magnetic coupling and/or a non-random distribution of Mn and Cr over the metal sub-lattice. The ferromagnetism seems to disappear for $t > \sim 0.9$ (for the ternary end composition $CrAs_{1-x}P_x$ Pauli paramagnetism is observed for $x > 0.07$[29]).

The temperature variation of the integrated intensity of the magnetic part of the 200 reflection (I_m) for $Mn_{0.98}Cr_{0.02}As_{0.88}P_{0.12}$ shows (Fig. 8) anomalous behaviour. This I_m versus T relationship should be compared with the corresponding one for $000^{\pm}$ in Fig. 7. The comparison brings out the fact that 200 has a ferromagnetic component even in the temperature region ($0\ K < T < T_{S1}$) for the H_a'-type magnetic order. The implication is accordingly that either the sample is in a (magnetic) two-phase state at the lowest temperatures or that H_a' and F modes co-exist. Moreover, Fig. 8 suggests an additional complication in that

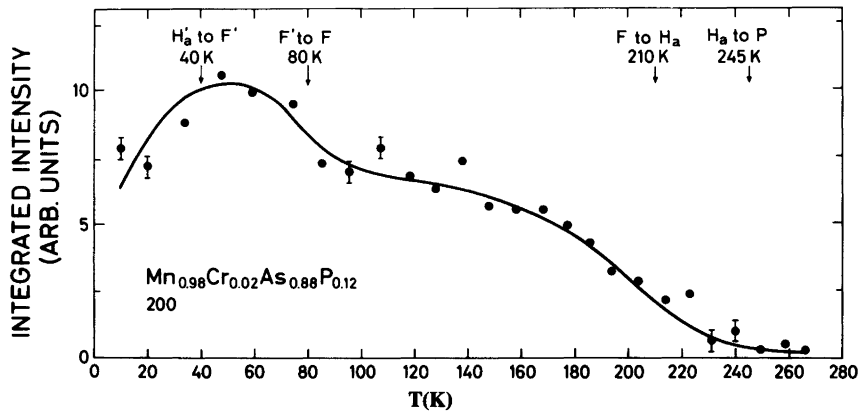

Fig. 8. Temperature dependence of the integrated intensity of the magnetic part of 200 for $Mn_{0.98}Cr_{0.02}As_{0.88}P_{0.12}$ between 10 and 270 K.

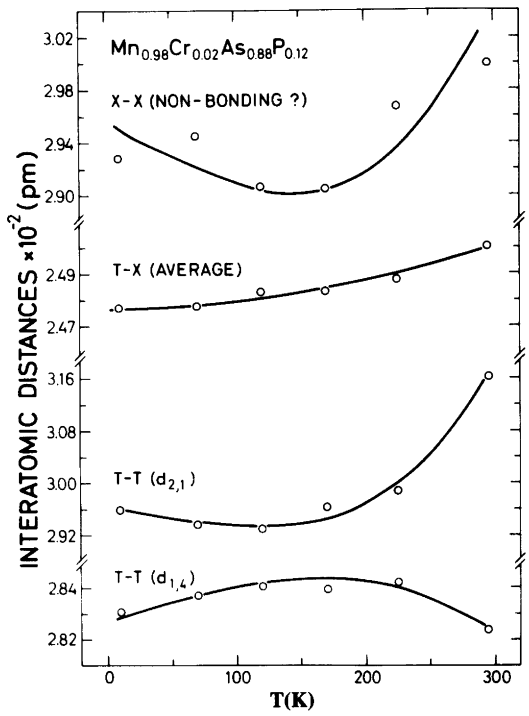

Fig. 9. Variation in selected interatomic distances with temperature between 10 and 300 K for $Mn_{0.98}Cr_{0.02}As_{0.88}P_{0.1.}$ $d_{1,4}$ and $d_{2,1}$ represent shortest and second shortest metal–metal (T–T) distances, T–X (average) denotes average of six shortest metal–non-metal distances and X–X (non-bonding?) reflects shortest non-metal–non-metal distance.

a turning of the spins of the ferromagnetic structure takes place at ~80 K. According to Rietveld refinements of the powder neutron diffraction data, the orientation of the ferromagnetic moments appears to change from being along the *b* axis (at low temperatures) to along the *a* axis.

The different complications made it difficult to deduce entirely reliable parameters for the ferro- and helimagnetic structures of $Mn_{0.98}Cr_{0.02}As_{0.88}P_{0.12}$. However, the values μ_H = 1.10±0.10 μ_B, $\tau_a/2\pi a^*$ = 0.073±0.001 and $\varphi_{1,2}$ = 56±8° for the H_a phase at 225 K and μ_F = 1.70±0.10 μ_B along *b* for the F phase at 70 K can be regarded as well established. Refinements in terms of the H_a model for the H_a'-type structure gave μ_H = 1.00±0.10 μ_B, $\tau_a/2\pi a^*$ = 0.071±0.001 and $\varphi_{1,2}$ = 48±10° at 10 K. The latter value for the magnetic moment is much smaller than the expected value of ~1.8 μ_B and this finding therefore lends additional support to the proposition (*vide supra*) that the present $Mn_{0.98}Cr_{0.02}As_{0.88}P_{0.12}$ sample is in a magnetic two-phase state (H_a' plus F, roughly half and half) at 0 K < T < T_{S1}. The magnetic two-phase phenomenon may originate from non-random distributions of Mn/Cr and As/P over the metal and non-metal sub-lattice, respectively. Similar findings were made for $Mn_{0.96}Cr_{0.04}As_{0.88}P_{0.12}$.

The temperature-induced changes in the interatomic distances of $Mn_{0.98}Cr_{0.02}As_{0.88}P_{0.12}$ below room temperature (Fig. 9) follow the same pattern as for $MnAs_{0.88}P_{0.12}$[7] and $MnAs_{0.90}P_{0.10}$[9] by exhibiting a concave shape towards the temperature axis for the shortest metal–metal distance ($d_{1,4}$) and a characteristic minimum in the second shortest metal–metal distance ($d_{2,1}$). These features are certainly associated with the magnetic P to H_a to F to H_a' transition sequence in $MnAs_{1-x}P_x$, but a microscopic interpretation cannot yet be advanced.

The total information available on the low-temperature magnetic properties of the quaternary MnAs–CrAs–CrP–MnP system, as obtained from powder X-ray and neutron diffraction data, magnetic susceptibility measurements and DTA data, are summarized in the form of the "phase diagram" in Fig. 1. Clearly, this diagram is incomplete with respect to the detailed positioning of the phase boundaries, but nevertheless brings out the extraordinary properties of $Mn_{1-t}Cr_tAs_{1-x}P_x$ where variation in the magnetic properties can be monitored by changes in *t* and *x*.

References

1. Fjellvåg, H. and Kjekshus, A. *Acta Chem. Scand., Ser. A 38* (1984) 1.
2. Fjellvåg, H. and Kjekshus, A. *Acta Chem. Scand., Ser. A 39* (1985) 671.
3. Andresen, A. F., Bärner, K., Fjellvåg, H., Heinemann, K., Kjekshus, A. and Sondermann, U. *J. Magn. Magn. Mater. 58* (1986) 287.
4. Andresen, A. F., Fjellvåg, H., Kjekshus, A. and Lebech, B. *J. Magn. Magn. Mater. 62* (1986) 247.
5. Komada, N., Westrum, E. F., Jr., Fjellvåg, H. and Kjekshus, A. *J. Magn. Magn. Mater. 65* (1987) 37.
6. Zięba, A., Fjellvåg, H. and Kjekshus, A. *J. Magn. Magn. Mater. 68* (1987) 115.
7. Fjellvåg, H., Andresen, A. F. and Bärner, K. *J. Magn. Magn. Mater. 46* (1984) 29.

8. Fjellvåg, H., Kjekshus, A. and Andresen, A. F. *J. Magn. Magn. Mater. 50* (1985) 287.
9. Fjellvåg, H., Kjekshus, A. and Stølen, S. *J. Solid State Chem. 64* (1986) 123.
10. Andresen, A. F., Fjellvåg, H., Steinsvoll, O., Kjekshus, A., Stølen, S. and Bärner, K. *J. Magn. Magn. Mater. 62* (1986) 241.
11. Fjellvåg, H., Grønvold, F., Kjekshus, A. and Stølen, S. *J. Phys. C20* (1987) 3005.
12. Labban, A. K., Westrum, E. F., Jr., Fjellvåg, H., Grønvold, F., Kjekshus, A. and Stølen, S. *J. Solid State Chem. 70* (1987) 185.
13. Rietveld, H. M. *J. Appl. Crystallogr. 2* (1969) 65.
14. Hewat, A. W. *The Rietveld Computer Program for the Profile Refinement of Neutron Diffraction Powder Patterns Modified for Anisotropic Thermal Vibrations,* UKAERE Harwell Report RRL 73/897, Harwell 1973.
15. Koester, L. and Yelon, W. B. In: Yelon, W. B., Ed., *Neutron Diffraction Newsletter,* The Neutron Diffraction Commission, Missouri 1983.
16. Watson, R. E. and Freeman, A. J. *Acta Crystallogr. 14* (1961) 27.
17. Roger, A. and Fruchart, R. *Mater. Res. Bull. 3* (1968) 253.
18. Suzuki, T. and Ido, H. *J. Phys. Soc. Jpn. 51* (1982) 3149.
19. Fjellvåg, H., Kjekshus, A., Andresen, A. F. and Zięba, A. *J. Magn. Magn. Mater. 61* (1986) 61.
20. Zięba, A., Zach, R., Fjellvåg, H. and Kjekshus, A. *J. Phys. Chem. Solids 48* (1987) 79.
21. Zięba, A., Selte, K., Kjekshus, A. and Andresen, A. F. *Acta Chem. Scand., Ser. A 32* (1978) 173.
22. Selte, K., Kjekshus, A., Andresen, A. F. and Zięba, A. *J. Phys. Chem. Solids 38* (1977) 719.
23. Haneda, S., Kazama, N., Yamaguchi, Y. and Watanabe, H. *J. Phys. Soc. Jpn. 42* (1977) 1212.
24. Hall, E. L., Schwartz, L. H., Felcher, G. P. and Ridgley, D. H. *J. Appl. Phys. 41* (1970) 939.
25. Ridgley, D. H. and Gleisman, J. H. *J. Appl. Phys. 39* (1968) 592.
26. Goodenough, J. B., Ridgley, D. H. and Newman, W. A. *Proc. Intern. Conf. Magnetism,* Nottingham 1964, p. 542.
27. Ido, H. *J. Phys. Soc. Jpn. 25* (1968) 1543.
28. Fjellvåg, H. and Kjekshus, A. *J. Solid State Chem. 59* (1985) 9.
29. Selte, K., Hjersing, H., Kjekshus, A., Andresen, A. F. and Fischer, P. *Acta Chem. Scand., Ser. A 29* (1975) 695.

Received November 9, 1987.